# Clinical Characterization of Host Response to Simian Hemorrhagic Fever Virus Infection in Permissive and Refractory Hosts: A Model for Determining Mechanisms of VHF Pathogenesis

Joseph P. Cornish,[a] Ian N. Moore,[b] Donna L. Perry,[c] Abigail Lara,*[c] Mahnaz Minai,[b] Dominique Promeneur[c], Katie R. Hagen,[c] Kimmo Virtaneva,[d] Monica Paneru,[d] Connor Buechler[e,f], David H. O'Connor[e,f], Adam L. Bailey[e,f,g] Kurt Cooper,[c] Steven Mazur,[c] John G. Bernbaum,[c] James Pettitt[c], Peter B. Jahrling,[a,c] Jens H. Kuhn,[c] Reed F. Johnson[a#]

[a]Emerging Viral Pathogens Section, Laboratory of Immunoregulation, Division of Intramural Research, National Institute of Allergy and Infectious Diseases, National Institutes of Health, Frederick, Maryland, USA

[b]Infectious Disease Pathogenesis Section, Comparative Medicine Branch, Division of Intramural Research, National Institute of Allergy and Infectious Diseases, National Institutes of Health, Rockville, Maryland, USA

[c]Integrated Research Facility, Division of Clinical Research, National Institute of Allergy and Infectious Diseases, National Institutes of Health, Frederick, Maryland, USA

[d]Genomics Unit, Research Technologies Branch, Rocky Mountain Laboratories, National Institute of Allergy and Infectious Diseases, National Institutes of Health, Hamilton, Montana, USA

[e]Department of Pathology and Laboratory Medicine, University of Wisconsin–Madison, Madison, Wisconsin 53711, USA.

[f]Wisconsin National Primate Research Center, Madison, Wisconsin 53711, USA.

[g]Current Affiliation: Department of Pathology and Immunology, Washington University in St. Louis School of Medicine, St. Louis, MO, 63110, USA.

[#]Address correspondence to Reed F. Johnson, johnsonreed@niaid.nih.gov

*Present address: One MedImmune Way, Gaithersburg, Maryland, USA

**ABSTRACT: 225/250**

**ARTICLE: 4729/5000**

**ABSTRACT** Simian hemorrhagic fever virus (SHFV) causes a fulminant and typically lethal viral hemorrhagic fever (VHF) in macaques (Cercopithecinae: *Macaca* spp.) but causes subclinical infections in patas monkeys (Cercopithecinae: *Erythrocebus patas*). This difference in disease course offers a unique opportunity to compare host-responses to infection by a VHF-causing virus in biologically similar susceptible and refractory animals. Patas and rhesus monkeys were inoculated side-by-side with SHFV. In contrast to the severe disease observed in rhesus monkeys, patas monkeys developed a limited clinical disease characterized by changes in complete blood counts, serum chemistries, and development of lymphadenopathy. Viremia was measurable 2 days after exposure and its duration varied by species. Infectious virus was detected in terminal tissues of both patas and rhesus monkeys. Varying degrees of overlap in changes in serum concentrations of IFN-γ, MCP-1, and IL-6 were observed between patas and rhesus monkeys, suggesting the presence of common and species-specific

cytokine responses to infection. Similarly, quantitative immunohistochemistry of terminal livers and whole blood flow cytometry revealed varying degrees of overlap in changes in macrophages, natural killer cells, and T-cells. The unexpected degree of overlap in host-response suggests that relatively small subsets of a host's response to infection may be responsible for driving pathogenesis that results in a hemorrhagic fever. Furthermore, comparative SHFV infection in patas and rhesus monkeys offers an experimental model to characterize host-response mechanisms associated with viral hemorrhagic fever and evaluate pan-viral hemorrhagic fever countermeasures.

**IMPORTANCE** Host-response mechanisms involved in pathogenesis of VHFs remain poorly understood. An underlying challenge is separating beneficial, inconsequential, and detrimental host-responses during infection. The comparison of host-responses to infection with the same virus in biologically similar animals that have drastically different disease manifestations allows for the identification of pathogenic mechanisms. SHFV, a surrogate virus for human VHF-causing viruses likely causes subclinical infection in African monkeys such as patas monkeys but can cause severe disease in Asian macaque monkeys. Data from the accompanying article by Buechler *et al*. support that infection of macaques and baboons with non-SHFV simarteviruses can establish persistent or long-term subclinical infections. Baboons, macaques, and patas monkeys are relatively closely taxonomically related (Cercopithecidae: Cercopithecinae) and therefore offer a unique opportunity to dissect how host-response differences determine disease outcome in VHFs.

**KEYWORDS** *Arteriviridae,* arterivirus, host-response, macaque, patas monkey, pathogenesis, SHFV, simartevirus, simian hemorrhagic fever, VHF, viral hemorrhagic fever

## INTRODUCTION

Viral hemorrhagic fevers (VHFs) are primarily caused by single-stranded RNA viruses (1). VHF is a broadly defined syndrome: fever, hepatic and renal complications, large increases in proinflammatory cytokines and coagulopathy are common features (2, 3). Simian hemorrhagic fever virus (SHFV) is a positive-sense, single-stranded RNA virus classified in the family *Arteriviridae*, which also includes equine arteritis virus and porcine reproductive and respiratory syndrome viruses 1 and 2 (4, 5). In addition to SHFV, several other simian arteriviruses (genus *Simartevirus*) have been identified (6-8). Among simarteviruses, SHFV, simian hemorrhagic encephalitis virus (SHEV), and Pebjah virus (PBJV) are known to cause severe disease in Asian macaques of various species (9). Kibale red colobus virus 1 (KRCV-1) was found to cause a self-limiting disease in crab-eating macaques (10). It is not known whether the other identified simarteviruses infect or cause disease in macaques or their natural hosts. Here, and in combination with accompanying article by Buechler *et al*., we examine infection of natural hosts (patas monkeys and baboons) with simarteviruses, and compare disease course of these simarteviruses in macaque monkeys.

SHFV was discovered during a VHF outbreak in National Institutes of Health (NIH) animal facilities in the United States in 1964 (11, 12). Transmission during the NIH

SHFV outbreak is thought to have occurred through tattooing needles used on both macaques and co-housed African primates (12). The virus is highly virulent in rhesus monkeys (*Macaca mulatta*), crab-eating macaques (*Macaca fasicularis*), stump-tailed macaques (*Macaca arctoides*), and Japanese macaques (*Macaca fuscata*), but SHFV causes little to no disease in African primates such as patas monkeys or baboons (11, 13, 14). SHFV infection in macaques mirrors aspects of human VHFs, such as Ebola virus disease, by inducing fever, edema, coagulopathy, hepatocellular degeneration and necrosis, and elevated inflammatory cytokine concentrations (13-15). Like all VHFs, simian hemorrhagic fever (SHF) is thought to be driven by a dysregulated host-response leading to a dysregulated immune response and poor viral clearance (13, 14, 16).

Studying SHFV offers a unique opportunity to compare infection and associated responses in refractory and highly susceptible primates that are biologically similar to each other and to humans. Some hemorrhagic fever-causing viruses naturally infect non-primate mammals that may serve as hosts or reservoirs. For instance, Marburg virus (*Filoviridae: Marburgvirus*, MARV) and Ravn virus (*Filoviridae: Marburgvirus*, RAVV) naturally circulate in Egyptian rousettes (*Rousettus aegyptiacus*), in which they do not cause disease, whereas these viruses cause frequently lethal disease experimentally in primates and naturally in humans (17). Similarly, arenaviruses associated with human VHFs, such as Machupo virus and Lassa virus (*Arenaviridae: Mammarenavirus*), subclinically infect distinct rodent reservoir hosts (18, 19). Comparing the response to infection between refractory hosts, preferably the reservoirs themselves, and susceptible hosts may offer significant insight into responses involved

in VHF pathogenesis. For most hemorrhagic fever-causing viruses, comparisons between refractory and susceptible animals during infection is confounded by large biological differences. For example, work with pathogenic mammarenaviruses has demonstrated that mechanisms present in murine hosts, even susceptible ones, are fundamentally different than those of primates (20). Unlike these examples, SHFV infects biologically similar refractory and susceptible animals and may provide a path towards meaningful interspecies comparisons of responses to hemorrhagic fever-causing virus infection.

The goal of this work was to compare host-responses in biologically similar nonhuman primates, patas (refractory) monkeys and rhesus (susceptible) monkeys, infected with SHFV to identify factors associated with differential outcomes to infection. The findings are the first in-depth characterization of SHFV infection in patas monkeys and confirm that patas monkeys are largely unaffected by SHFV infection. Our work demonstrates that, although patas and rhesus monkeys develop drastically different diseases, the host-responses to infection overlap, and suggest that VHF pathogenesis may be driven by a relatively small subset of the overall host-response to infection.

## RESULTS

**Simian hemorrhagic fever virus (SHFV) infection results in mild clinical disease.** Twelve monkeys were grouped by species into SHFV-inoculated and PBS inoculated groups, n=3 per. Inoculations were 1-ml intramuscular injections in the right quadriceps. The 3 SHFV-inoculated patas monkeys developed axillary and inguinal

lymphadenopathy starting on day 10 post-inoculation (PI) that persisted until the conclusion of the experiment at 21 days PI. The 3 SHFV-inoculated rhesus monkeys developed severe disease. Two subjects ("non-survivors") met clinical endpoint criteria and were euthanized on days 8 and 11 post-inoculation. The third subject ("survivor") survived until the conclusion of the experiment (day 20 PE). Signs of disease were first detectable on day 4 PI SHFV-inoculated rhesus monkeys developed a range of clinical signs and included: gingival bleeding (1/3 subjects), inguinal lymphadenopathy (1/3), and axillary lymphadenopathy (2/3). All SHFV-inoculated rhesus monkeys developed petechial rashes and axial and inguinal lymphadenopathy by their respective endpoints. All 3 SHFV-inoculated rhesus monkeys developed tremors and motor dysfunction by day 6 PI that remained until each subject's respective endpoint. The non-surviving rhesus monkeys developed facial edema that began on day 8 PI that persisted to their respective endpoints. The surviving SHFV-inoculated rhesus monkey developed facial edema that began on day 12 PI and resolved by day 16 PI. All mock-inoculated rhesus appeared clinically normal and displayed no outward signs of disease throughout the experiment.

**SHFV infection results in clinical pathology changes in patas monkeys.** In SHFV-inoculated patas monkeys, alanine aminotransferase (ALT), alkaline phosphatase (ALP) and aspartate aminotransferase (AST) concentrations were elevated on day 4 PI and remained above baseline until the end of the experiment (Fig 1A-C). γ-glutamyl transferase (GGT) concentrations remained normal in all SHFV-inoculated patas monkeys (Fig 1D). SHFV-inoculated rhesus monkeys showed similar trends except that GGT concentrations rose starting on day 4 PI. ALP, AST, and GGT

concentrations remained elevated in the surviving SHFV-inoculated rhesus monkey until the conclusion of the experiment, whereas ALT returned to baseline concentrations. Although changes in serum chemistries were observed in all SHFV-inoculated subjects, values did not reach concentrations suggestive of a severe clinical disease. All subjects experienced decreases in albumin concentration coinciding with globulin concentration increases (Fig 1F) on day 8 and day 4 PI in SHFV-inoculated patas and rhesus monkeys, respectively. Reticulocyte counts decreased in both SHFV-inoculated patas and rhesus monkeys: on day 6 PI in patas monkeys and on day 4 PI in rhesus monkeys (Fig 1E), but did not drop below the normal range. Hematocrit (HCT) remained normal in all subjects except for the surviving SHFV-inoculated rhesus where HCT decreased starting on day 10 PI with anemia persisting to study end (Fig 1G). Albumin concentrations (Fig 1H) began decreasing in SHFV inoculated patas monkeys on day 6 PI to day 8 PI after which concentrations remained depressed till the conclusion of the study. In SHFV-inoculated rhesus monkeys, albumin concentrations began decreasing on day 2 and continued to decrease in all subjects till their respective endpoints. No significant changes in serum chemistry were observed in mock-inoculated patas and rhesus monkeys.

Complete blood counts revealed minor decreases in lymphocyte numbers early in all SHFV-inoculated patas and rhesus monkeys, followed by a return to baseline counts at day 8 PI (Fig 1I). Lymphocyte counts increased in the surviving rhesus, but the mechanism is not known at this time and may represent further maturation of the immune response. Monocyte counts decreased slightly in all SHFV-inoculated patas and rhesus monkeys on day 2 PI before increasing by day 6 PI. After day 6 PI

monocyte counts (Fig 1J) in SHFV-inoculated patas monkeys returned to baseline by day 15 followed by a second increase in 2/3 subjects. Unlike the patas monkeys, monocyte counts in SHFV-inoculated rhesus monkeys continued to increase until each subject's endpoint. No significant changes were observed in complete blood counts in any mock-inoculated subjects.

**SHFV infection causes mild pathology in patas monkeys.** Gross examination of SHFV-inoculated patas monkeys during necropsy confirmed peripheral lymphadenopathy in all three subjects, but there were no other remarkable findings. Non-surviving SHFV-inoculated rhesus monkeys had marked hepatosplenomegaly: hepatic tissues were friable and firm. Moderate peripheral and visceral lymphadenopathy was found in both non-surviving rhesus monkeys, whereas moderate peripheral lymphadenopathy was the only significant finding in the surviving rhesus monkey. The kidneys of one non-surviving SHFV-inoculated rhesus monkey contained multiple infarctions with severe renal hemorrhage and necrosis. No significant gross lesions were observed in either mock-inoculated group.

Histopathological examination of the spleen in SHFV-inoculated patas monkeys revealed abundant plasma cells in one subject. The spleens of the 2 remaining SHFV-inoculated patas monkeys were within normal limits. The livers of two SHFV-inoculated patas monkeys had minimal inflammatory changes, whereas that of the third patas monkey was within normal limits. Hyperplasia was evident in the inguinal lymph nodes of 1 SHFV-inoculated patas monkey. The spleens of SHFV-inoculated rhesus monkeys were different in each subject: in the two non-survivors, one was congested, whereas fibrin deposition was evident in the other. The spleen of the surviving subject exhibited

changes that were consistent with reactive lymphoid hyperplasia, characterized by diffuse expansion and proliferation of B-cells at the margins of each follicle. Each of the livers of SHFV-inoculated rhesus monkeys were also histologically different. In the survivor, perivascular inflammation with multifocal areas of necrosis were evident. The major finding in the liver of one non-survivor was vacuolated hepatocytes, whereas rare thrombi were the major observation in the remaining non-survivor. Hyperplasia was present in inguinal lymph nodes of all three SHFV-inoculated rhesus monkeys. Tissues of all mock-inoculated subjects were normal apart from vascular congestion in 2 patas monkey spleens. While all three SHFV-inoculated rhesus monkeys displayed neurological signs, on histopathological examination CNS tissues did not reveal any evidence of vasculitis or other changes that would suggest encephalitis. CNS tissues of all mock-inoculated animals and SHFV-inoculated patas monkeys were found to be within normal histologic limits. Upon histopathological examination kidneys of all subjects appeared to be within normal histologic limits.

Immunohistochemical staining used to detect ionized calcium-binding adaptor 1 (Iba-1)-expressing macrophages revealed morphologically-normal macrophages in the livers of all 3 SHFV-inoculated patas monkeys. In contrast, the livers of all 3 SHFV-inoculated rhesus monkeys contained macrophages that were often rounded and contained a diffusely vacuolated cytoplasm (Fig 2A, inset). These changes in macrophage morphology were in direct contrast to these cells in infected patas monkeys which often exhibited a more stellate shape and cytoplasm that was diffusely dark brown when evaluated immunohistochemically. Similar findings were seen in the inguinal lymph nodes and spleen of SHFV-inoculated patas and rhesus monkeys, although rounded

223 macrophages were detected in the spleen of one SHFV-inoculated patas monkey and
224 inguinal lymph nodes of a second SHFV-inoculated patas monkey. Macrophages
225 appeared morphologically normal in all mock-inoculated subjects.

226 **Viremia is sustained in SHFV-infected patas monkeys.** SHFV-inoculated patas
227 and rhesus monkeys became viremic on day 2 PI (Fig 3A). The average peak titers in
228 patas and rhesus monkeys were 6.75 (range 6.41–6.96) and 7.08 (range 6.79–7.36)
229 $\log_{10}$ viral RNA (vRNA) copies per ml, respectively. Viremia peaked on day 4 PI in patas
230 monkeys and was detectable in all three subjects for the remainder of the experiment,
231 except for days 15 and 19 PI where viremia was below the limit of detection in two
232 subjects. Terminal viremia in SHFV-inoculated patas monkeys was 3.42 (range 2.51–
233 4.43) $\log_{10}$ vRNA copies per ml. In SHFV-inoculated rhesus monkeys, viremia peaked
234 between days 5 and 12 PI. Terminal viremia in SHFV-inoculated rhesus was 6.30, 7.36
235 and 4.17 $\log_{10}$ vRNA copies per mL in the two non-survivors and single survivor,
236 respectively.

237 SHFV was detected by plaque assay in the axillary lymph node (n=1), spleen (n=1),
238 and jejunum (n=1) of 2 SHFV-inoculated patas monkeys (Fig 3B). The highest titer was
239 3.36 $\log_{10}$ PFU/mg in the jejunum of the SHFV-inoculated patas with the highest
240 terminal viremia. In the 2 non-surviving SHFV-inoculated rhesus monkeys, SHFV was
241 found in axillary and inguinal lymph nodes (n=2 and 1, respectively), spleen (n=2), liver
242 (n=2), jejunum (n=1), thyroid (n=2), brain-stem (n=1), and kidney (n=2). Only the kidney
243 of the surviving SHFV-inoculated rhesus monkey contained SHFV, and its titer (2.53
244 $\log_{10}$ PFU/mg) was similar to those of the two non-survivors (2.82 and 5.35 $\log_{10}$

PFU/mg, respectively). The highest tissue titer in SHFV-inoculated rhesus monkeys was 4.27 $\log_{10}$ PFU/mg in axillary lymph nodes.

Bone marrow, cerebella, jejuna, axial and inguinal lymph nodes, kidneys, and thyroids were assessed for evidence of SHFV infection by TEM. DMVs and apparently mature virions were found in the jejunum of the SHFV-inoculated patas monkey with the highest terminal viremia (Fig 3C and D). ISH for SHFV vRNA was performed to assess the livers, spleens, brainstems, cerebella, and femoral bone marrow of SHFV-inoculated subjects for signs of SHFV replication. The liver of 2 SHFV-inoculated patas monkeys and, rarely, the spleen of the third was positive for SHFV vRNA (Fig 2B) using RNAscope. The femoral bone marrow of the patas monkey with the highest terminal titer was positive for vRNA. vRNA was detected by ISH in the cerebellum, brain-stem, spleen, and liver of all SHFV-inoculated rhesus monkeys. vRNA was detected in femoral bone marrow of all three SHFV-inoculated rhesus monkeys. Morphologically, ISH data support that monocytes and endothelial cells are sites of SHFV infection in examined livers, spleens, brainstems, and cerebella of both SHFV-inoculated patas and rhesus monkeys. In all tissues, cells positive for SHFV vRNA (RNAScope) were morphologically consistent with macrophage-lineage cells; in each of the tissues evaluated these cells were present in fairly low numbers.

**SHFV infection of patas and rhesus monkeys elicit strong and overlapping immune responses.** Quantitative immunohistochemistry (qIHC) revealed statistically significant (t-test, $p<0.05$) changes in inflammatory cell populations in livers of SHFV-inoculated monkeys (Fig 4A). On average, SHFV-inoculated patas monkeys had livers with increased CD3 and Iba1 signals when compared to uninfected patas monkeys.

CD8 signals were increased in the liver of SHFV-inoculated patas monkeys when compared to uninfected patas monkeys but did not reach significance (p=0.06). CD8 and NKG2A signals were increased in SHFV-inoculated rhesus monkeys compared to uninfected controls. In the spleen, significant changes were seen in major histocompatibility complex class-1 (MHC1) and Iba1 signals between SHFV-inoculated and mock-inoculated patas monkeys (Fig 4B). No significant differences in cell concentrations were observed for CD3, CD8, and NKG2A in the splenic tissue of infected and uninfected patas monkeys. No significant changes were seen between SHFV-inoculated and mock-inoculated rhesus monkey spleens for any of the markers quantified.

Interferon gamma (IFN-γ) concentrations in all SHFV-inoculated patas monkeys were elevated on day 2 PI compared to the pre-exposure mean concentration (group mean fold change (GMFC): 55.52, group mean concentration (GMC): 87.24 pg/ml) (Fig 4A). Later IFN-γ concentrations decreased to baseline in 2 SHFV-inoculated patas monkeys, whereas the concentration of the third patas monkey remained elevated throughout the experiment with a second peak in concentration at 12 days PI (group mean fold change (GMFC): 29.75; GMC: 43.11 pg/ml). The two non-surviving SHFV-inoculated rhesus monkeys had peak concentrations of similar magnitudes 2 days PI (GMFC: 14.57; GMC: 83.09 pg/ml) and all three subjects had increased concentrations by day 6 PI (GMFC: 20.58; GMC: 99.93 pg/ml).

Mean monocyte chemoattractant protein 1 (MCP-1) concentrations peaked at day 2 PI in all SHFV-inoculated patas monkeys and the two non-surviving rhesus monkeys (28.61 and 38.80 group MFC, respectively; 11,477.68 and 8,266.47 pg/ml GMC,

291 respectively) (Fig 4B). All SHFV-inoculated rhesus monkeys had a second MCP-1
292 concentration peak at day 8 PI (group MFC: 50.68; GMC: 5,617.24 pg/ml).

293 SHFV-inoculated patas monkeys had mild increases in interleukin 6 (IL-6)
294 concentrations in comparison to their mock counterparts (3.93 and 1.07 mean of
295 individual PI fold changes respectively, 11.04 and 3.97 pg/ml GMC, respectively).
296 SHFV-inoculated rhesus monkeys had increased IL-6 concentrations 2 days PI (group
297 MFC: 17.34; GMC: 55.02 pg/ml) and the two non-survivors on their respective terminal
298 days (419.82-fold change, 2,637.57 pg/ml non-survivor group mean concentration) (Fig
299 4E). The remaining analytes were below the limit of detection and were not considered
300 for further analysis.

301 Flow cytometry of whole blood revealed increased numbers of circulating natural
302 killer (NK) cells in SHFV-inoculated patas monkeys on days 12 and 19 PI (Fig 5A). In
303 contrast, SHFV-inoculated rhesus monkeys had a single, larger, increase in circulating
304 NK cells on day 8 PI. Changes in $Ki67^+$ NK cells in SHFV-inoculated patas monkeys
305 were more variable, with one patas monkey reaching peak numbers at 2 days PI and
306 the other two patas monkeys reaching peak numbers of day 8 PI (Fig 5B). Increased Ki-
307 $67^+$ numbers in the surviving rhesus monkey returned to baseline by the conclusion of
308 the experiment.

309 Circulating $CD14^+$ monocytes were decreased in SHFV-inoculated patas monkeys at
310 day 2 PI prior to returning to baseline counts, whereas counts in SHFV-inoculated
311 rhesus monkeys appeared unchanged throughout the experiment (Fig 5C). SHFV-
312 inoculated patas and rhesus monkeys had decreased numbers of $CD14^+$ $CD163^+$
313 macrophages (Fig 5D) starting at day 2 PI that remained until each subject's respective

endpoint. Both SHFV-inoculated patas and rhesus monkeys had declines in circulating $CD4^+$ and $CD8^+$ T-cell numbers starting on day 2 PI, but counts recovered by day 10 PI (data not shown). Numbers of PD-$1^+$ $CD8^+$ T-cells began to increase in both SHFV-inoculated patas and rhesus monkeys on day 10 and 8 PI, respectively, and remained elevated until the conclusion of the experiment (Fig 6E). Ki-$67^+$ $CD8^+$ T-cell numbers were elevated on day 2 PI before decreasing to baseline counts. A second, larger, peak in Ki-$67^+$ $CD8^+$ T-cell numbers was seen on day 8 PI in both SHFV-inoculated patas and rhesus monkeys, followed again by a return to baseline counts (Fig 5F).

IgG antibody responses were detected by enzyme-linked immunosorbent assay (ELISA) in all three SHFV-inoculated patas monkeys and two of the three (the survivor and one non-survivor) SHFV-inoculated rhesus monkeys (Fig 6). Two SHFV-inoculated patas monkeys had detectable anti-SHFV antibodies on day 10 PI and the third on day 15 PI. The two SHFV-inoculated rhesus monkeys with a response began responding on day 10 PI. Response magnitude continued to increase in all responding subjects till their respective endpoints. Anti-SHFV antibodies were not detected in mock-inoculated subjects at any time.

## DISCUSSION

The goal of this study was to characterize SHFV infection of patas monkeys in comparison to rhesus monkeys to assess the usefulness of comparing biologically similar refractory and susceptible primates of different species in hemorrhagic fever virus infection. This is the first report of successful experimental SHFV infection of patas monkeys and further characterizes SHFV in rhesus monkeys.

Our data demonstrate that SHFV can replicate to high titers in patas monkeys without causing significant disease. Consistent with previously obtained data derived from experimentally SHFV-infected macaques (10, 13, 14), ISH and electron microscopy of infected tissues indicate that tissue-resident macrophages and endothelial cells are likely the main targets of SHFV in patas monkeys. Although not definitive, our findings indicate that SHFV may replicate in the same or similar cell populations in both patas and rhesus monkeys. Additional experiments are required to confirm the tissue distribution of SHFV and characterize the infected cell types over the course of the infection.

The immune response of SHFV-inoculated patas monkeys is similar to that of SHFV-inoculated rhesus monkeys and includes initial lymphopenia and monocytopenia, elevated IFN-γ and MCP-1 concentrations, and changes in circulating macrophage, NK, and T-cell populations. Patas monkeys did not react with IL-6 concentration increases to SHFV infection, whereas increased IL-6 concentrations in SHFV infected rhesus were observed in this experiment and have been previously reported (10, 13, 14). This difference is of particular interest as IL-6 has been associated with non-survival in SHFV-infected rhesus monkeys, and because decreased concentrations of IL-6 were seen in *in vitro* infection of monocyte-derived macrophages and dendritic cells from baboons (13, 15). Given the potential role of IL-6 in human VHFs, our model offers an opportunity to explore the potential of therapies, such as neutralizing antibodies, aimed at modulating IL-6 responses during infection.

IFN-γ may be a more challenging target given that concentrations fluctuated in both patas and rhesus monkeys and that observed differences were largely temporal. Future

359 experiments are required to determine whether the difference in IFN-γ responses
360 between patas and rhesus monkeys is indicative of functional differences of NK or T-
361 cells during SHFV infection. IFN-γ has been implicated in conflicting roles in other VHF-
362 causing virus infections, such as filovirus and mammarenavirus infections, ranging from
363 detrimental to protective (21-26). If differences exist between activation states of NK or
364 T-cells between animals of different species, further characterization of relevant
365 cytokine concentrations and cell-cell interactions is warranted. Given the temporal
366 nature of the differences in IFN-γ, a more prudent therapeutic approach may be to
367 directly stimulate or inhibit dysfunctional cell-types through supplementing factors or
368 inhibiting signaling.

369 Livers of SHFV-inoculated patas monkeys had increased CD3 and Iba1 signals
370 whereas those of SHFV-inoculated rhesus monkeys had elevated CD8 and NKG2A
371 signals. Increases in CD8 and NKG2A signals in the absence of an increase in CD3
372 signal suggests that SHFV infection leads to an increase in infiltrating NK cells in rhesus
373 monkeys (27). Indeed, the numbers of circulating NK cells were elevated at day 8 PI.
374 Although there were clear quantitative differences in tissue and circulating NK cells
375 between SHFV-infected patas and rhesus monkeys, all animals were affected by similar
376 changes in circulating Ki-67$^{+}$ NK cell numbers. The data suggest that a potent type 1
377 interferon response occurs in SHFV-inoculated rhesus monkeys, but it is unclear
378 whether a similar response is present in SHFV-inoculated patas monkeys. NK cell
379 responses are important for survival in human Ebola virus disease cases (28, 29).
380 Differences in the timing of NK cell responses are a key difference in non-lethal, mild
381 disease and lethal, severe (Lassa virus) infections in macaques (30), suggesting the

382 species-specific NK cell responses observed here warrant further exploration. For
383 comparison, and as described in the accompanying paper by Buechler *et al*., olive
384 baboons and rhesus monkeys infected with SWBV-1 also developed increases in NK
385 and $CD8^+$ T-cell numbers, with $CD8^+$ T-cell numbers remaining elevated through the
386 observation period. NK cell dynamics suggest a short-lived peak in olive baboons and
387 rhesus monkeys that did not develop severe disease due to SWBV-1 infection.
388 Together, these data support a role for appropriate timing and activation of NK cells in
389 modulating disease presentation in VHFs.

390 Increased detection of Iba1, a macrophage marker, suggests that SHFV infection
391 leads to an increase in the number of macrophages in the liver (31). Determining the
392 sources of these additional liver macrophages in SHFV-inoculated patas monkeys is
393 important given the changes in MCP-1 concentrations and the differential roles of
394 hepatic resident and non-resident macrophages (32-35). SHVF is dependent on CD163
395 for cellular entry (36), and preferential targeting of $CD163^+$ cells by SHFV may explain
396 why both patas and rhesus monkeys lost $CD163^+$ macrophages. CD163 is associated
397 with alternatively-polarized macrophages and macrophage polarization has a significant
398 role in immunity and infection (37-39). Additionally, the presence of rounded and
399 vacuolated macrophages in the livers of SHFV-inoculated rhesus monkeys but not their
400 patas counter parts suggests and active response to infection and that tissue-resident
401 macrophages may play a key role in SHFV pathogenesis. Future serial-sampling
402 studies will be required to fully characterize tissue-specific immune responses over the
403 course of SHFV infection, but will be challenging since the disease is not uniformly
404 lethal.

Consistent with the complete blood counts, flow cytometry revealed early decreases in both $CD4^+$ and $CD8^+$ T-cells supporting the presence of lymphopenia in both patas and rhesus monkeys. Interestingly, on day 2 PI, both SHFV-inoculated patas and rhesus monkeys had an increase in Ki-$67^+$ $CD8^+$ T-cell numbers, suggesting some level of proliferation was present even in the face of depletion (40, 41). On days 8 and 10 PI, $CD8^+$ T-cell counts returned to baseline in all monkeys. This return coincided with a second spike in Ki-$67^+$ $CD8^+$ counts and the start of an elevated count of PD-$1^+$ $CD8^+$ T-cells. PD-1 is associated with T-cell exhaustion and is also found on activated T-cells (42, 43). PD-$1^+$ T-cells and $CD8^+$ T-cells appear to play important roles in human cases of Ebola virus disease (28, 29, 44-46). Consequently, it may be fruitful to determine if SHFV provides a means for studying the role of T-cell dysfunction in EVD. As SHFV is capable of infecting antigen-presenting cells, it will be important to determine if poor T-cell responses during SHFV infection are due to deficits in antigen presentation as is suspected to be the case during Ebola virus infection in humans and non-human primates (21, 46-50). T-cell exhaustion has also been implicated in chronic viral infections and may be an important mechanism in the development of persistent SHFV infections in patas monkeys (43). Given the extreme differences in disease course and outcomes during SHFV infection in patas and rhesus monkeys the relatively high degree of overlap in host-response features was unexpected. Changes in IFN-γ and MCP-1 concentrations, and circulating macrophage, NK, and T-cell populations were similar between SHFV-inoculated patas and rhesus monkeys. Interestingly, viral loads were largely similar between all monkeys and ISH data suggests that SHFV targets the same cell types in cercopithecines. Our data suggests that when biologically similar

primates of two species are infected with the same pathogen that host responses are initially quite similar however, as the virus interacts with the host to modulate the immune response, the effectiveness of the immune response is diminished, likely as a result of the degree of adaptation to the host.

Rather than a “cytokine storm”, we propose that a process driven by NK cells and macrophages is the deciding factor in developing hemorrhagic fever, either alone, or through their impacts on otherwise beneficial or seemingly inconsequential host-responses. Ultimately, the differences in disease course in SHFV patas and rhesus monkeys are due to their biological differences, ranging from organism-level physiology to minute genotypic differences. Although biologically similar, patas and rhesus monkeys are distinct species. A core drawback of the approach taken in the paper is that although it is relatively simple to catalogue host-responses in monkeys of two species, it is difficult to contextualize them. Without extensive characterization, it is challenging to determine which impact a given host-response has on members of each species: clear differences may have no impact on disease whereas topically similar responses may have divergent functional impacts.

However, as a tool for identifying host-response mechanisms as targets for medical countermeasures against viral hemorrhagic fevers, the issue of biological differences may become more tractable. Interactions between cell-cell and cell-SHFV interactions may be driven by highly-specific mechanics and are therefore far more difficult to translate or target. On the other hand, the resulting functional differences are more readily targetable. For example, it may be that the large differences in IL-6 concentrations between patas and rhesus monkeys observed in this work are driven by

451 SHFV-infected macrophages. Rather than attempting to navigate the convolutions of
452 species-specific macrophage biology, targeting IL-6-producing macrophages, IL-6, or
453 the IL-6 receptor offer far more direct paths to identifying druggable targets. Under the
454 macrophage/IL-6 example and in the context of identifying targets for therapeutic
455 development, the minutiae of species-specific macrophage biology may be rather
456 unimportant when the results of those biologies suggest a common target.

457 A top down approach to more fully characterize SHFV infection in patas and rhesus
458 monkeys will streamline identification of host components or sub-systems that are
459 sources of responses that result in VHF. Identification of and targeting the high-level
460 responses could ultimately even result in pan-VHF therapeutics.

461

462 **MATERIALS AND METHODS**

463 **Cells and Virus.** Simian hemorrhagic fever virus (SHFV; *Nidovirales: Arteriviridae:*
464 *Simartevirus: Simian hemorrhagic fever virus*) strain LVR42-0/M6941 (51) was
465 passaged twice before a final passage on MA-104 cells to create the virus stock. Briefly,
466 virus stock was prepared by freeze-thawing infected cells three times prior to
467 clarification with low-speed centrifugation and was then concentrated by centrifugation
468 at 16,000xg. Pellets were resuspended in PBS and combined. The final viral stock was
469 sequenced as in (52) for quality control purposes (GenBank accession number
470 pending). Sequencing confirmed the expected genotype and lack of any contamination.

471 **Animals.** Six patas monkeys (4 females and 2 males) and 6 rhesus monkeys (3
472 females and 3 males) where used in this study. Patas monkeys ranged from 5.51–14.01

kg in weight and 9–14 years in age, whereas rhesus monkeys ranged from 4.77–12.75 kg in weight and 8–12 years in age. Rhesus monkeys were obtained from the National Institute of Allergy and Infectious Disease (NIH/NIAID) rhesus monkey colony. Patas monkeys were obtained from the National Institute of Child Health and Human Development (NIH/NICHD). Subjects were screened for simian T-lymphotrophic virus, simian immunodeficiency virus, and simian retrovirus infections, and cleared for use in the experiment by the facility veterinarian. Patas monkeys were determined to be serologically negative for SHFV prior to enrollment. Rhesus monkeys were obtained from a SHFV-free source, and therefore were not screened prior to use in this experiment. Subjects were randomly assigned to 4 groups (2 groups of patas monkeys, inoculated and mock-inoculated, and 2 groups of rhesus monkeys, inoculated and mock-inoculated), for sex, age and weight. The animals of one group of patas monkeys and 1 group of rhesus monkeys each received 5,000 PFU of SHFV diluted in 1 ml of PBS, whereas the animals of the remaining groups each received 1 ml of PBS (mock) by intramuscular injection of the right quadriceps. Subjects were housed in separate rooms and had access to food and water *ad libitum*.

Subjects were monitored at least twice daily. Physical exams were performed on pre-determined experimental days (-9, -6, 0, 2, 4, 6, 8, 10, 12, 15, 19, and 21) and prior to euthanasia. Blood was collected on all physical exam days, except day 0, and prior to euthanasia. Scheduled days for euthanasia with necropsy were as follows: mock-inoculated patas monkeys at 19 days post-inoculation, SHFV-inoculated patas monkeys at 21 days post-inoculation, mock-inoculated rhesus monkeys at 10 days post-inoculation, and SHFV-inoculated rhesus monkeys at 20 days post-inoculation. Subjects

were euthanized at scheduled times or upon reaching pre-established clinical endpoint criteria including overall clinical appearance, respiratory function, responsiveness, and core body temperature. At euthanasia, subjects were perfused with saline before necropsy and sample collection. Subjects were housed in an AAALAC, International, accredited facility under biosafety level 4 (BSL-4) conditions due to the nature of the facility in which the experiments were performed. All experimental procedures were approved by the NIAID DCR Animal Care and Use Committee and were performed in compliance with the Animal Welfare Act regulations, Public Health Service policy, and the Guide for the Care and Use of Laboratory Animals recommendations.

**Virus Quantification**. Virus stock and tissue concentrations were determined by plaque assay on MA-104 cells. Briefly, serial dilutions of 10% (w/v) tissue homogenates were added to cell monolayers and incubated for 1 h. Then, monolayers were overlaid with 0.8% tragacanth (Sigma, St. Louse, MO), MEM (Lonza, Walkersville, MD), 1% penicillin-streptomycin (Lonza) and 2% heat-inactivated fetal bovine serum (Sigma) final concentration. After a 3-day incubation, overlays were aspirated, and monolayers fixed using 10% neutral-buffered formalin (Fisher Scientific, Hampton, TN) with 0.2% crystal violet (Ricca, Arlington, TC) prior to enumeration.

**Plasma Cytokines.** Plasma concentrations of granulocyte-macrophage colony stimulating factor (GM-CSF), interferon gamma (IFN-γ), macrophage chemoattractant protein 1 (MCP-1), vascular endothelium growth factor (VEGF), and interleukins 2, 4, 6, 8, 10, and 17 were measured using a Milliplex non-human primate kit (MilliporeSigma, St Louis, MO) as described previously (13).

**Hematology**. Complete blood counts (Sysmex XS1000i, Lincolnshire, IL) and selected serum chemistries using Piccolo General Chemistry 13 kits (Abaxis, Union City, CA) were performed at the described timepoints using blood collected in K3 EDTA and SST tubes (BD, San Jose, CA). Due to a lack of published data, standard ranges for patas monkeys were defined as the mean +/- two standard deviations of all pre-exposure timepoints. Standard ranges for rhesus monkeys were determined from data kept by veterinary staff on subjects housed in the facility.

**Histology, *In Situ* Hybridization, and Immunohistochemistry.** Formalin-fixed paraffin-embedded (FFPE) animal tissue sections (5 µm) were used for immunohistochemical staining using the following antibodies: NKG2A (Abcam, Cambridge, MA); Iba1 (Wako, Richmond, VA); MHC1 [Clone EPR1394Y] (Abcam); CD8 (Abcam); CD3 [Clone 12] (AbD, Serotec Hercules, CA). Staining was performed on the Bond RX platform (Leica Biosystems) according to the manufacturer's protocol. Briefly, sections were baked, deparaffinized, and rehydrated. Epitope retrieval was performed using Leica Epitope Retrieval Solution 1, pH 6.0, heated to 100°C for 20 min, and quenched with hydrogen peroxide prior to addition of primary antibody. The Bond Polymer Refine Detection kit (Leica Biosystems) was used for chromogen detection. Image analysis was performed on select tissues from all groups to quantify the degree of positive staining. Images were obtained on a bright-field Leica Aperio AT2 slide scanner (Leica Biosystems) and processed using Aperio Image Scope [v12.3] algorithms. The Positive Pixel Count Algorithm was used to assign pixels to intensity ranges for positive (strong ($n_{sp}$), medium ($n_p$), and weak ($n_{wp}$)) and negative ($n_n$) pixels.

Pixels were categorized, and positive percentage was calculated per image as a fraction of the number of strong positive ($n_{sp}$) pixel to the total number of stained pixels:

$$\%_{positive} = \frac{n_{sp}}{n_{total}} * 100 = \frac{n_{sp}}{(n_{sp} + n_p + n_{wp} + n_n)} * 100$$

SHFV RNA RNAscope *in situ* hybridization (ISH) was performed as previously described (53).

**Electron Microscopy.** Electron microscopy samples were processed and imaged as previously reported (54).

**qPCR viremia.** Monkey peripheral blood samples were inactivated in 3 volumes of Trizol LS buffer (Thermo Fisher Scientific, Waltham, MA) and RNA was extracted using the Qiagen AllPrep 96 kit as described by manufacturer (Qiagen, Valencia, CA) except that each sample was treated with 27 units of DNAse I (Qiagen). SHFV RNA copy number was determined by RT-qPCR using primers and probes targeting the SHFV gp15 nucleocapsid gene. The AgPath-ID One-Step RT-PCR kit (Thermo Fisher Scientific) was used to perform the assay. Primers and Cal Fluor Orange 560/BHQ1 labeled probe were synthetized by LCG Biosearch Technologies (Petaluma, CA). RT-qPCR reactions were performed in 20-µl reactions using forward primer (5'-CGACCTCCGAGTTGTTCTACCT-3'), reverse primer (5'-GCCTCCGTTGTCGTAGTACCT-3'), and fluorescent probe (5'-CCCACCTCAGCACACATCAAACAGCT-3'). Synthetic DNA (5'-TTTCGCCGAACCCGGCGACCTCCGAGTTGTTCTACCTGGTCCCACCTCAGCACACATCAAACAGCTGCTGATCAGGTACTACGACAACGGAGGCGGAAATCTTTCATATG-3'; LCG Biosearch Technologies, Novato, CA) was used as a standard. The qPCR

562 reactions were run at 50 °C for 10 min, 95 °C for 10 min, 55 cycles of 95 °C for 15 s,
563 and 60 °C for 45 s on a 7900HT Fast Real-Time PCR System (Thermo Fisher
564 Scientific). Data were analyzed using Applied Biosystems 7900HT Fast Real-Time PCR
565 System Software (Thermo Fisher Scientific).

566 **Flow Cytometry.** Whole blood was assessed for the following markers: HLA-DR-
567 FITC (BioLegend, San Diego, CA), CD16-APC (BD), PD-1-APC-Cy7 (BioLegend), CD3-
568 AF700 (BD), CD11c-PE (BD), CD28-PE-Cy5 (BioLegend), NKG2a-PE-Cy7 (Beckman
569 Coulter, Brea CA), CD163-PE/Dazzle594 (BioLegend), CD4-BV421 (BD), CD14-BV510
570 (BioLegend), CD20-BV570 (BioLegend), CD8a-BV605 (BD), CD123-BV650 (BD), PD-
571 L1-BV711 (BioLegend), CD95-BV785 (BioLegend), and Ki-67-PerCP-Cy5.5 (BD).
572 Briefly, 100 µl of whole blood was incubated with 100 µl of the marker panel (excluding
573 Ki-67) and incubated for 20 min. Red blood cells were lysed with 1 ml of BD FACSLyse
574 (BD) for 10 min. Cells were washed and fixed for 30 min using BD Cytofix/Cytoperm
575 (BD) and incubated with Ki-67 antibody for 30 min at 4° C, followed by a final wash in
576 1xBD Permwash (BD). Data acquisition and analysis was performed with FlowJo
577 version 10.2 (BD).

578 **Enzyme-linked immunosorbent Assays.** Lysates from MA-104 cells infected with
579 SHVF or mock infected (media only) were used as substrates. Immulon 2 HB
580 microplates (Thermo Fisher Scientific, Walkersville, MD) were coated with cell lysates
581 diluted in PBS and incubated overnight at 4◦C. Plates were then washed five times with
582 wash buffer comprised of PBS/0.2% Tween 20 and blocked for 2 h at room temperature
583 with 5% nonfat milk (LabScientific, Highlands, NJ, USA) dissolved in PBS. Plates were
584 then washed five times with wash buffer, and analyte serum diluted at 1:50 in PBS/2.5%

585 milk/0.05% Tween 20 was added in duplicate to corresponding wells. After a 1-h
586 incubation at room temperature, plates were washed and horseradish peroxidase-
587 conjugated anti-monkey IgG (Sigma Aldrich, St. Louis, MO, USA; A2054) was added.
588 Plates were then incubated for 1 h at room temperature before washing with wash
589 buffer and adding TMB Substrate (Thermo Fisher Scientific, Walkersville, MD, USA).
590 Following a 10-min incubation, 100 µl of TMB stop solution (Thermo Fisher Scientific,
591 Walkersville, MD, USA) were added to each well and the plates were read on a
592 SpectraMax Plus 384 plate reader (Molecular Devices, Sunnyvale, CA, USA) at 450 nm.

593 **Acknowledgments**

594 This work, in part, was supported by the NIAID Division of Intramural Research and
595 the NIAID Division of Clinical Research via the Battelle Memorial Institute's prime
596 contract with the National Institute of Allergy and Infectious Diseases (NIAID) at the
597 National Institutes of Health, under contract no. HHSN272200700016I (DP, KRHP, SM,
598 JGB, JHK.

599 We would like to thank the entire EVPS and IRF-Frederick staff for their support of
600 the experiments. We especially would like to thank Tim Cooper (IRF-Frederick) for his
601 help in establishing standard ranges for complete blood counts and serum chemistries.
602 We also would like to thank Laura Bollinger and Jiro Wada (IRF-Frederick) for technical
603 writing services and figure preparation, respectively.

604

605 **Figure Legends**

606 **Fig 1:** Alanine aminotransferase (A), alkaline phosphatase (B), aspartate
607 aminotransferase (C), gamma-glutamyltransferase (D), reticulocyte number (E), globulin
608 (F), hematocrit (HCT) (G), albumin (H), lymphocyte number (I), monocyte number (J)
609 values for patas monkeys (orange lines) and rhesus monkeys (blue lines) either
610 inoculated with 5,000 PFU of SHFV (open symbols) or with PBS (closed symbols).
611 Shaded regions represent standard range of all pre-exposure values for patas monkeys
612 or previously collected values for rhesus monkeys. Data represent means of each
613 group.

614 **Fig 2:** Representative images of liver immunohistochemistry for Iba1 in livers of
615 mock- and SHFV-inoculated patas and rhesus monkeys; inset images highlight
616 macrophage morphology for each group (A). Representative images of *in situ*
617 hybridization for SHFV viral RNA in terminal cerebellum, brain stem, spleen, femoral
618 bone marrow and liver samples from patas and rhesus monkeys inoculated with SHFV
619 (B).

620 **Fig 3:** Mean viremia values in viral RNA copies per ml of whole blood for mock (solid
621 symbols) and SHFV-inoculated (open symbols) patas monkeys (orange) and rhesus
622 monkeys (blue) (A). Mean titer of tissues for SHFV-inoculated patas monkeys (orange)
623 and rhesus monkeys (blue) in PFU per mg of 10% tissue homogenate (B, Lymph Node
624 (LN)). Electron micrograph of jejunum from a SHFV-inoculated patas monkey showing
625 double-membrane vesicles (C). Electron micrograph of jejunum from a SHFV-inoculated
626 patas monkey showing apparently mature virions (yellow arrowheads) (D).

627 **Fig 4:** Mean quantitative immunohistochemistry values of indicated marker in mock-
628 and SHFV-inoculated patas and rhesus monkey livers and spleens (A, B). Mean plasma

629 concentrations in pg per ml of indicated analyte for mock (closed symbols) and SHFV-
630 inoculated (open symbols) patas monkeys (orange) and rhesus monkeys (blue) (C–E).
631 Gray lines represent the lower and upper limits of quantitation (LLOQ and ULOQ,
632 respectively).

633 **Fig 5:** Mean percentage of indicated cell populations from whole blood of mock
634 (closed symbols) and SHFV-inoculated (open symbols) patas monkeys (orange) and
635 rhesus monkeys (blue) (A-F).

636 **Fig 6:** Mean ELISA absorbance values for patas monkeys (orange) and rhesus
637 monkeys (blue) either inoculated with 5,000 PFU of SHFV (open symbols) or with PBS
638 (closed symbols).

639

640 **References**

641 1. **Singh SK, Ruzek D (ed).** 2013. Viral Hemorrhagic Fevers. Taylor &
642 Francis/CRC Press, Boca Raton, USA.
643 2. **Kuhn JH, Clawson AN, Radoshitzky SR, Wahl-Jensen V, Bavari S, Jahrling**
644 **PB.** 2013. Viral hemorrhagic fevers: history and definitions, p 3–13. *In* Singh SK,
645 Ruzek D (ed), Viral hemorrhagic fevers doi:10.1201/b15172-3. Taylor &
646 Francis/CRC Press, Boca Raton, USA.
647 3. **Paessler S, Walker DH.** 2013. Pathogenesis of the viral hemorrhagic fevers.
648 Annu Rev Pathol **8:**411-440.
649 4. **Faaberg KS, Balasuriya UB, Brinton MA, Gorbalenya AE, Leung FC-C,**
650 **Nauwynck H, Snijder EJ, Stadejek T, Yang H, Yoo D.** 2011. Family

*Arteriviridae*. *In* King AMQ, Adams MJ, Carstens EB, Lefkowitz EJ (ed), Virus taxonomy—Ninth Report of the International Committee on Taxonomy of Viruses. Elsevier/Academic Press, London, UK.

5. **Kuhn JH, Lauck M, Bailey AL, Shchetinin AM, Vishnevskaya TV, Bào Y, Ng TFF, LeBreton M, Schneider BS, Gillis A, Tamoufe U, Diffo JLD, Takuo JM, Kondov NO, Coffey LL, Wolfe ND, Delwart E, Clawson AN, Postnikova E, Bollinger L, Lackemeyer MG, Radoshitzky SR, Palacios G, Wada J, Shevtsova ZV, Jahrling PB, Lapin BA, Deriabin PG, Dunowska M, Alkhovsky SV, Rogers J, Friedrich TC, O'Connor DH, Goldberg TL.** 2016. Reorganization and expansion of the nidoviral family *Arteriviridae*. Arch Virol **161:**755–768.

6. **Bailey AL, Lauck M, Sibley SD, Pecotte J, Rice K, Weny G, Tumukunde A, Hyeroba D, Greene J, Correll M, Gleicher M, Friedrich TC, Jahrling PB, Kuhn JH, Goldberg TL, Rogers J, O'Connor DH.** 2014. Two novel simian arteriviruses in captive and wild baboons (*Papio* spp.). J Virol **88:**13231-13239.

7. **Lauck M, Sibley SD, Hyeroba D, Tumukunde A, Weny G, Chapman CA, Ting N, Switzer WM, Kuhn JH, Friedrich TC, O'Connor DH, Goldberg TL.** 2013. Exceptional simian hemorrhagic fever virus diversity in a wild African primate community. J Virol **87:**688-691.

8. **Gravell M, London WT, Leon M, Palmer AE, Hamilton RS.** 1986. Elimination of persistent simian hemorrhagic fever (SHF) virus infection in patas monkeys. Proc Soc Exp Biol Med **181:**219-225.

673 9. **Lauck M, Alkhovsky SV, Bào Y, Bailey AL, Shevtsova ZV, Shchetinin AM,**
674 **Vishnevskaya TV, Lackemeyer MG, Postnikova E, Mazur S, Wada J,**
675 **Radoshitzky SR, Friedrich TC, Lapin BA, Deriabin PG, Jahrling PB,**
676 **Goldberg TL, O'Connor DH, Kuhn JH.** 2015. Historical outbreaks of simian
677 hemorrhagic fever in captive macaques were caused by distinct arteriviruses. J
678 Virol **89:**8082-8087.
679 10. **Wahl-Jensen V, Johnson JC, Lauck M, Weinfurter JT, Moncla LH, Weiler**
680 **AM, Charlier O, Rojas O, Byrum R, Ragland DR, Huzella L, Zommer E,**
681 **Cohen M, Bernbaum JG, Caì Y, Sanford HB, Mazur S, Johnson RF, Qin J,**
682 **Palacios GF, Bailey AL, Jahrling PB, Goldberg TL, O'Connor DH, Friedrich**
683 **TC, Kuhn JH.** 2016. Divergent simian arteriviruses cause simian hemorrhagic
684 fever of differing severities in macaques. MBio **7:**e02009-02015.
685 11. **Tauraso NM, Shelokov A, Palmer AE, Allen AM.** 1968. Simian hemorrhagic
686 fever. III. Isolation and characterization of a viral agent. Am J Trop Med Hyg
687 **17:**422-431.
688 12. **Palmer AE, Allen AM, Tauraso NM, Shelokov A.** 1968. Simian hemorrhagic
689 fever. I. Clinical and epizootiologic aspects of an outbreak among quarantined
690 monkeys. Am J Trop Med Hyg **17:**404-412.
691 13. **Johnson RF, Dodd LE, Yellayi S, Gu W, Cann JA, Jett C, Bernbaum JG,**
692 **Ragland DR, St Claire M, Byrum R, Paragas J, Blaney JE, Jahrling PB.** 2011.
693 Simian hemorrhagic fever virus infection of rhesus macaques as a model of viral
694 hemorrhagic fever: clinical characterization and risk factors for severe disease.
695 Virology **421:**129-140.

14. **Vatter HA, Donaldson EF, Huynh J, Rawlings S, Manoharan M, Legasse A, Planer S, Dickerson MF, Lewis AD, Colgin LMA, Axthelm MK, Pecotte JK, Baric RS, Wong SW, Brinton MA.** 2015. A simian hemorrhagic fever virus isolate from persistently infected baboons efficiently induces hemorrhagic fever disease in Japanese macaques. Virology **474:**186-198.

15. **Vatter HA, Brinton MA.** 2014. Differential responses of disease-resistant and disease-susceptible primate macrophages and myeloid dendritic cells to simian hemorrhagic fever virus infection. J Virol **88:**2095-2106.

16. **Smith DR, Holbrook MR, Gowen BB.** 2014. Animal models of viral hemorrhagic fever. Antiviral Res **112:**59-79.

17. **Amman BR, Swanepoel R, Nichol ST, Towner JS.** 2017. Ecology of filoviruses. Curr Top Microbiol Immunol **411:**23-61.

18. **Radoshitzky SR, Kuhn JH, Jahrling PB, Bavari S.** 2018. Hemorrhagic fever-causing mammarenaviruses, p 517-545. *In* Bozue J, Cote CK, Glass PJ (ed), Medical aspects of biological warfare. Borden Institute, US Army Medical Department Center and School, Health Readiness Center of Excellence, Fort Sam Houston, Texas, USA.

19. **Radoshitzky SR, Bào Y, Buchmeier MJ, Charrel RN, Clawson AN, Clegg CS, DeRisi JL, Emonet S, Gonzalez J-P, Kuhn JH, Lukashevich IS, Peters CJ, Romanowski V, Salvato MS, Stenglein MD, de la Torre JC.** 2015. Past, present, and future of arenavirus taxonomy. Arch Virol **160:**1851–1874.

20. **Vela E.** 2012. Animal models, prophylaxis, and therapeutics for arenavirus infections. Viruses **4:**1802-1829.

719 21. **Hutchinson KL, Rollin PE.** 2007. Cytokine and chemokine expression in
720 humans infected with Sudan Ebola virus. J Infect Dis **196 Suppl 2:**S357-363.
721 22. **Rhein BA, Powers LS, Rogers K, Anantpadma M, Singh BK, Sakurai Y, Bair**
722 **T, Miller-Hunt C, Sinn P, Davey RA, Monick MM, Maury W.** 2015. Interferon-γ
723 inhibits Ebola virus infection. PLoS Pathog **11:**e1005263.
724 23. **Wauquier N, Becquart P, Padilla C, Baize S, Leroy EM.** 2010. Human fatal
725 Zaire Ebola virus infection is associated with an aberrant innate immunity and
726 with massive lymphocyte apoptosis. PLoS Negl Trop Dis **4:**e837.
727 24. **Asper M, Sternsdorf T, Hass M, Drosten C, Rhode A, Schmitz H, Günther S.**
728 2004. Inhibition of different Lassa virus strains by alpha and Ggmma interferons
729 and comparison with a less pathogenic arenavirus. J Virol **78:**3162-3169.
730 25. **Kolokoltsova OA, Yun NE, Poussard AL, Smith JK, Smith JN, Salazar M,**
731 **Walker A, Tseng C-TK, Aronson JF, Paessler S.** 2010. Mice lacking alpha/beta
732 and gamma interferon receptors are susceptible to Junin virus infection. J Virol
733 **84:**13063-13067.
734 26. **Patterson M, Seregin A, Huang C, Kolokoltsova O, Smith J, Miller M, Smith**
735 **J, Yun N, Poussard A, Grant A, Tigabu B, Walker A, Paessler S.** 2014.
736 Rescue of a recombinant Machupo virus from cloned cDNAs and *in vivo*
737 characterization in interferon (αβ/γ) receptor double knockout mice. J Virol
738 **88:**1914-1923.
739 27. **Verstrepen BE, Fagrouch Z, van Heteren M, Buitendijk H, Haaksma T,**
740 **Beenhakker N, Palù G, Richner JM, Diamond MS, Bogers WM, Barzon L,**
741 **Chabierski S, Ulbert S, Kondova I, Verschoor EJ.** 2014. Experimental

infection of rhesus macaques and common marmosets with a European strain of West Nile virus. PLoS Negl Trop Dis **8:**e2797.

28. **Liu X, Speranza E, Muñoz-Fontela C, Haldenby S, Rickett NY, Garcia-Dorival I, Fang Y, Hall Y, Zekeng E-G, Lüdtke A, Xia D, Kerber R, Krumkamp R, Duraffour S, Sissoko D, Kenny J, Rockliffe N, Williamson ED, Laws TR, N'Faly M, Matthews DA, Günther S, Cossins AR, Sprecher A, Connor JH, Carroll MW, Hiscox JA.** 2017. Transcriptomic signatures differentiate survival from fatal outcomes in humans infected with Ebola virus. Genome Biol **18:**4.

29. **Cimini E, Viola D, Cabeza-Cabrerizo M, Romanelli A, Tumino N, Sacchi A, Bordoni V, Casetti R, Turchi F, Martini F, Bore JA, Koundouno FR, Duraffour S, Michel J, Holm T, Zekeng EG, Cowley L, Garcia Dorival I, Doerrbecker J, Hetzelt N, Baum JHJ, Portmann J, Wölfel R, Gabriel M, Miranda O, Díaz G, Díaz JE, Fleites YA, Piñeiro CA, Castro CM, Koivogui L, Magassouba NF, Diallo B, Ruibal P, Oestereich L, Wozniak DM, Lüdtke A, Becker-Ziaja B, Capobianchi MR, Ippolito G, Carroll MW, Günther S, Di Caro A, Muñoz-Fontela C, Agrati C.** 2017. Different features of Vδ2 T and NK cells in fatal and non-fatal human Ebola infections. PLoS Negl Trop Dis **11:**e0005645.

30. **Rasmussen AL, Tchitchek N, Safronetz D, Carter VS, Williams CM, Haddock E, Korth MJ, Feldmann H, Katze MG.** 2015. Delayed inflammatory and cell death responses are associated with reduced pathogenicity in Lujo virus-infected cynomolgus macaques. J Virol **89:**2543-2552.

31. **Utans U, Arceci RJ, Yamashita Y, Russell ME.** 1995. Cloning and characterization of allograft inflammatory factor-1: a novel macrophage factor

765 identified in rat cardiac allografts with chronic rejection. J Clin Invest **95:**2954-
766 2962.
767 32. **Baeck C, Wei X, Bartneck M, Fech V, Heymann F, Gassler N, Hittatiya K,**
768 **Eulberg D, Luedde T, Trautwein C, Tacke F.** 2014. Pharmacological inhibition
769 of the chemokine C-C motif chemokine ligand 2 (monocyte chemoattractant
770 protein 1) accelerates liver fibrosis regression by suppressing Ly-6C$^+$
771 macrophage infiltration in mice. Hepatology **59:**1060-1072.
772 33. **Heymann F, Peusquens J, Ludwig-Portugall I, Kohlhepp M, Ergen C,**
773 **Niemietz P, Martin C, van Rooijen N, Ochando JC, Randolph GJ, Luedde T,**
774 **Ginhoux F, Kurts C, Trautwein C, Tacke F.** 2015. Liver inflammation abrogates
775 immunological tolerance induced by Kupffer cells. Hepatology **62:**279-291.
776 34. **Karlmark KR, Weiskirchen R, Zimmermann HW, Gassler N, Ginhoux F,**
777 **Weber C, Merad M, Luedde T, Trautwein C, Tacke F.** 2009. Hepatic
778 recruitment of the inflammatory Gr1$^+$ monocyte subset upon liver injury promotes
779 hepatic fibrosis. Hepatology **50:**261-274.
780 35. **Ramachandran P, Pellicoro A, Vernon MA, Boulter L, Aucott RL, Ali A,**
781 **Hartland SN, Snowdon VK, Cappon A, Gordon-Walker TT, Williams MJ,**
782 **Dunbar DR, Manning JR, van Rooijen N, Fallowfield JA, Forbes SJ, Iredale**
783 **JP.** 2012. Differential Ly-6C expression identifies the recruited macrophage
784 phenotype, which orchestrates the regression of murine liver fibrosis. Proc Natl
785 Acad Sci U S A **109:**E3186-3195.
786 36. **Caì Y, Postnikova EN, Bernbaum JG, Yú SQ, Mazur S, Deiuliis NM,**
787 **Radoshitzky SR, Lackemeyer MG, McCluskey A, Robinson PJ, Haucke V,**

788 **Wahl-Jensen V, Bailey AL, Lauck M, Friedrich TC, O'Connor DH, Goldberg**
789 **TL, Jahrling PB, Kuhn JH.** 2015. Simian hemorrhagic fever virus cell entry is
790 dependent on CD163 and uses a clathrin-mediated endocytosis-like pathway. J
791 Virol **89:**844-856.
792 37. **Lasky CE, Olson RM, Brown CR.** 2015. Macrophagem polarization during
793 murine Lyme borreliosis. Infect Immun **83:**2627-2635.
794 38. **Marino S, Cilfone NA, Mattila JT, Linderman JJ, Flynn JL, Kirschner DE.**
795 2015. Macrophage polarization drives granuloma outcome during *Mycobacterium*
796 *tuberculosis* infection. Infect Immun **83:**324-338.
797 39. **Murray PJ, Wynn TA.** 2011. Protective and pathogenic functions of macrophage
798 subsets. Nat Rev Immunol **11:**723-737.
799 40. **Scholzen T, Gerdes J.** 2000. The Ki-67 protein: from the known and the
800 unknown. J Cell Physiol **182:**311-322.
801 41. **Shedlock DJ, Talbott KT, Morrow MP, Ferraro B, Hokey DA, Muthumani K,**
802 **Weiner DB.** 2010. Ki-67 staining for determination of rhesus macaque T cell
803 proliferative responses *ex vivo*. Cytometry A **77:**275-284.
804 42. **Hong JJ, Amancha PK, Rogers K, Ansari AA, Villinger F.** 2013. Re-evaluation
805 of PD-1 expression by T cells as a marker for immune exhaustion during SIV
806 infection. PLoS One **8:**e60186.
807 43. **Jin H-T, Anderson AC, Tan WG, West EE, Ha S-J, Araki K, Freeman GJ,**
808 **Kuchroo VK, Ahmed R.** 2010. Cooperation of Tim-3 and PD-1 in CD8 T-cell
809 exhaustion during chronic viral infection. Proc Natl Acad Sci U S A **107:**14733-
810 14738.

811 44. **Agrati C, Castilletti C, Casetti R, Sacchi A, Falasca L, Turchi F, Tumino N,**
812 **Bordoni V, Cimini E, Viola D, Lalle E, Bordi L, Lanini S, Martini F, Nicastri E,**
813 **Petrosillo N, Puro V, Piacentini M, Di Caro A, Kobinger GP, Zumla A,**
814 **Ippolito G, Capobianchi MR.** 2016. Longitudinal characterization of
815 dysfunctional T cell-activation during human acute Ebola infection. Cell Death Dis
816 **7:**e2164.
817 45. **McElroy AK, Akondy RS, Davis CW, Ellebedy AH, Mehta AK, Kraft CS, Lyon**
818 **GM, Ribner BS, Varkey J, Sidney J, Sette A, Campbell S, Ströher U, Damon**
819 **I, Nichol ST, Spiropoulou CF, Ahmed R.** 2015. Human Ebola virus infection
820 results in substantial immune activation. Proc Natl Acad Sci U S A **112:**4719-
821 4724.
822 46. **Ruibal P, Oestereich L, Lüdtke A, Becker-Ziaja B, Wozniak DM, Kerber R,**
823 **Korva M, Cabeza-Cabrerizo M, Bore JA, Koundouno FR, Duraffour S, Weller**
824 **R, Thorenz A, Cimini E, Viola D, Agrati C, Repits J, Afrough B, Cowley LA,**
825 **Ngabo D, Hinzmann J, Mertens M, Vitoriano I, Logue CH, Boettcher JP,**
826 **Pallasch E, Sachse A, Bah A, Nitzsche K, Kuisma E, Michel J, Holm T,**
827 **Zekeng E-G, García-Dorival I, Wölfel R, Stoecker K, Fleischmann E,**
828 **Strecker T, Di Caro A, Avsic-Zupanc T, Kurth A, Meschi S, Mely S, Newman**
829 **E, Bocquin A, Kis Z, Kelterbaum A, Molkenthin P, Carletti F, Portmann J, et**
830 **al.** 2016. Unique human immune signature of Ebola virus disease in Guinea.
831 Nature **533:**100-104.
832 47. **Bosio CM, Aman MJ, Grogan C, Hogan R, Ruthel G, Negley D,**
833 **Mohamadzadeh M, Bavari S, Schmaljohn A.** 2003. Ebola and Marburg viruses

834 replicate in monocyte-derived dendritic cells without inducing the production of
835 cytokines and full maturation. J Infect Dis **188:**1630-1638.
836 48. **Ilinykh PA, Lubaki NM, Widen SG, Renn LA, Theisen TC, Rabin RL, Wood**
837 **TG, Bukreyev A.** 2015. Different temporal effects of Ebola virus VP35 and VP24
838 proteins on global gene expression in human dendritic cells. J Virol **89:**7567-
839 7583.
840 49. **Menicucci AR, Versteeg K, Woolsey C, Mire CE, Geisbert JB, Cross RW,**
841 **Agans KN, Jankeel A, Geisbert TW, Messaoudi I.** 2017. Transcriptome
842 analysis of circulating immune cell subsets highlight the role of monocytes in
843 Zaire Ebola virus Makona pathogenesis. Front Immunol **8:**1372.
844 50. **Lubaki NM, Younan P, Santos RI, Meyer M, Iampietro M, Koup RA,**
845 **Bukreyev A.** 2016. The Ebola interferon inhibiting domains attenuate and
846 dysregulate cell-mediated immune responses. PLoS Pathog **12:**e1006031.
847 51. **Lauck M, Palacios G, Wiley MR, Lǐ Y, Fāng Y, Lackemeyer MG, Caì Y, Bailey**
848 **AL, Postnikova E, Radoshitzky SR, Johnson RF, Alkhovsky SV, Deriabin**
849 **PG, Friedrich TC, Goldberg TL, Jahrling PB, O'Connor DH, Kuhn JH.** 2014.
850 Genome sequences of simian hemorrhagic fever virus variant NIH LVR42-
851 0/M6941 isolates (*Arteriviridae*: *Arterivirus*). Genome Announc **2:**e00978-00914.
852 52. **Cornish JP, Diaz L, Ricklefs SM, Kanakabandi K, Sword J, Jahrling PB,**
853 **Kuhn JH, Porcella SF, Johnson RF.** 2017. Sequence of Reston virus isolate
854 AZ-1435, an ebolavirus isolate obtained during the 1989-1990 Reston virus
855 epizootic in the United States. Genome Announc **5:**S757-760.

856 53. **Yú SQ, Caì Y, Lyons C, Johnson RF, Postnikova E, Mazur S, Johnson JC,**
857 **Radoshitzky SR, Bailey AL, Lauck M, Goldberg TL, O'Connor DH, Jahrling**
858 **PB, Friedrich TC, Kuhn JH.** 2016. Specific detection of two divergent simian
859 arteriviruses using RNAscope *in situ* hybridization. PLoS One **11:**e0151313.
860 54. **Perry DL, Huzella LM, Bernbaum JG, Holbrook MR, Jahrling PB, Hagen KR,**
861 **Schnell MJ, Johnson RF.** 2018. Ebola virus localization in the macaque
862 reproductive tract during acute Ebola virus disease. Am J Pathol **188:**550-558.

863

Figure 1

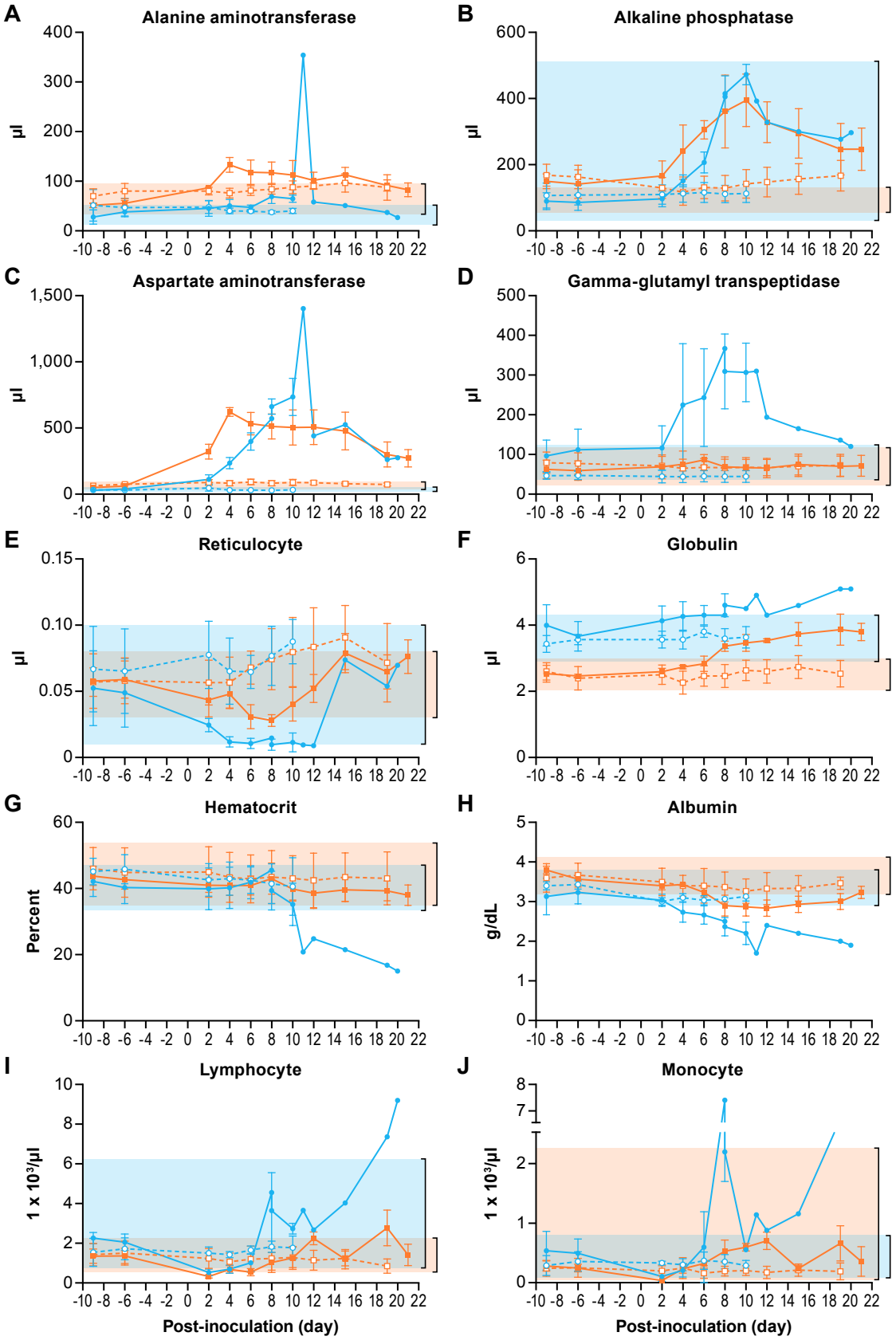


**Figure 1.** Alanine aminotransferase (A), alkaline phosphatase (B), aspartate aminotransferase (C), gamma-glutamyltransferase (D), reticulocyte number (E), globulin (F), hematocrit (HCT) (G), albumin (H), lymphocyte number (I), monocyte number (J) values for patas monkeys (orange lines) and rhesus monkeys (blue lines) either inoculated with 5,000 PFU of SHFV (solid symbols) or with PBS (open symbols). Shaded regions represent standard range of all pre-exposure values for patas monkeys or previously collected values for rhesus monkeys. Data represent means of each group.

Figure 2

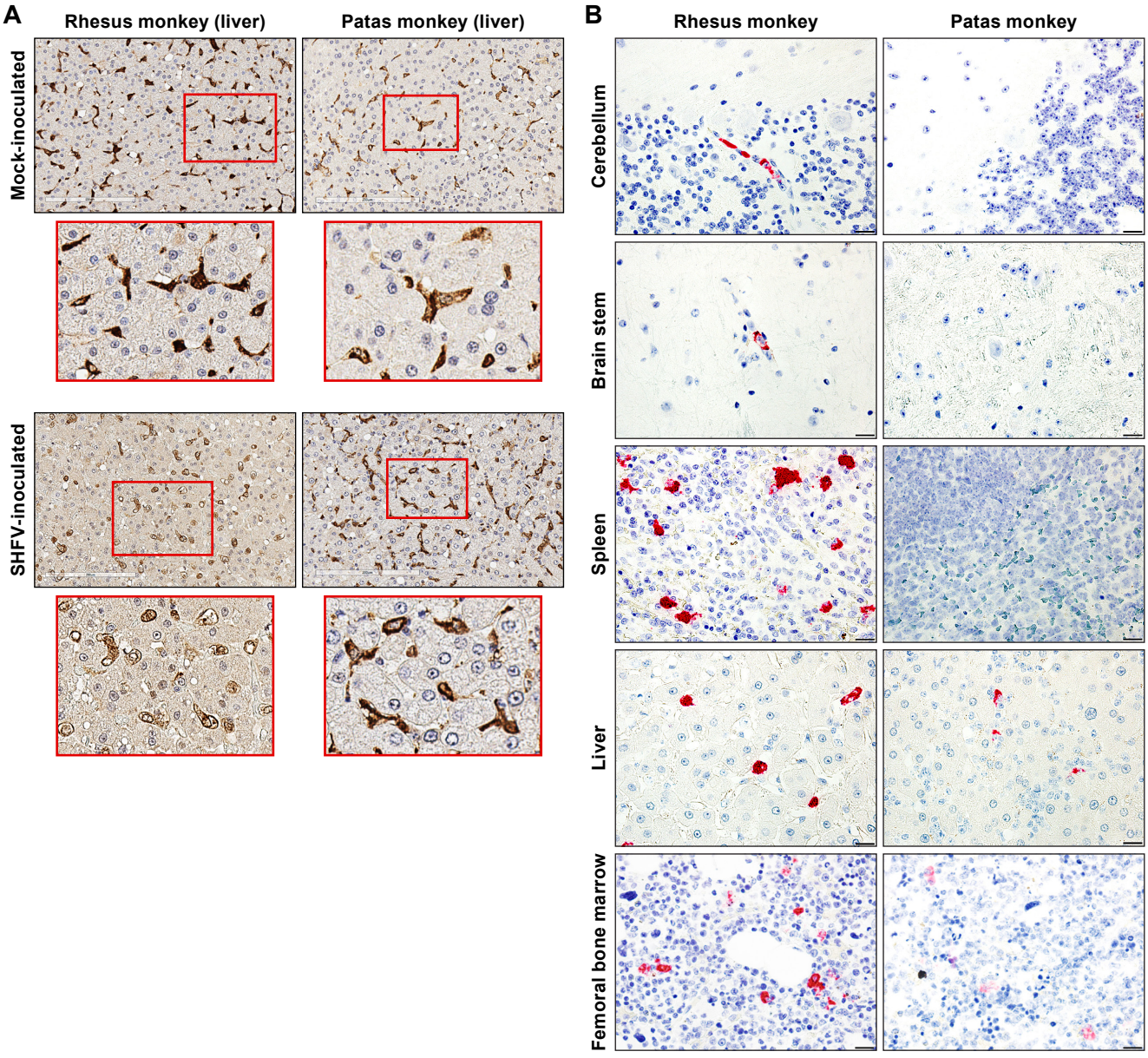


**Figure 2.** Representative images of liver immunohistochemistry for Iba1 in livers of mock- and SHFV-inoculated patas and rhesus monkeys; inset images highlight macrophage morphology for each group (A). Representative images of *in situ* hybridization for SHFV viral RNA in terminal cerebellum, brain stem, spleen, femoral bone marrow and liver samples from patas and rhesus monkeys inoculated with SHFV (B).

Figure 3

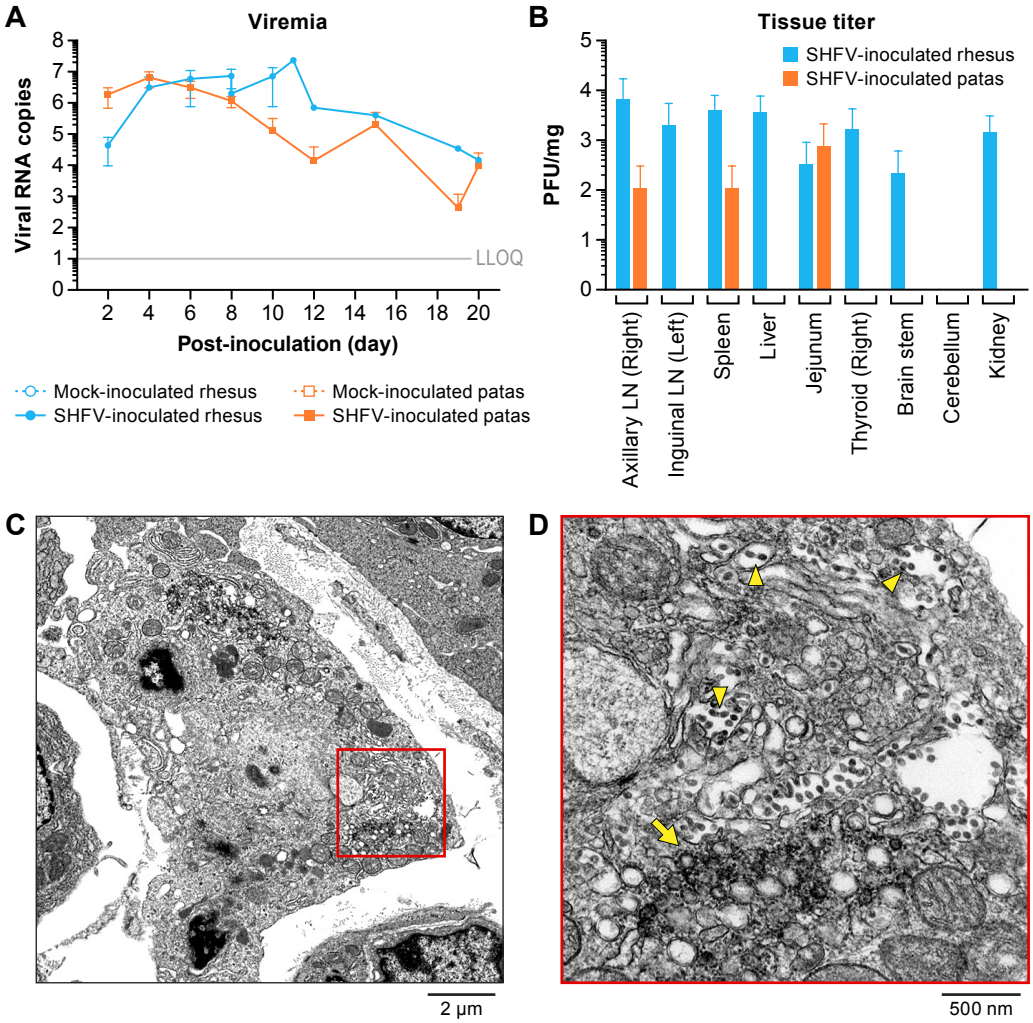


**Figure 3.** Mean viremia values in viral RNA copies per ml of whole blood for mock (open symbols) and SHFV-inoculated (solid symbols) patas (orange) and rhesus (blue) monkeys (A). Mean titer of tissues for SHFV-inoculated patas (orange) and rhesus (blue) monkeys in PFU per mg of 10% tissue homogenate (B, Lymph Node (LN)). Electron micrograph of jejunum from a SHFV-inoculated patas monkey showing double-membrane vesicles and mature virions (C). Electron micrograph of jejunum from a SHFV-inoculated patas monkey showing apparently mature virions (yellow arrowheads) (D).

Figure 4

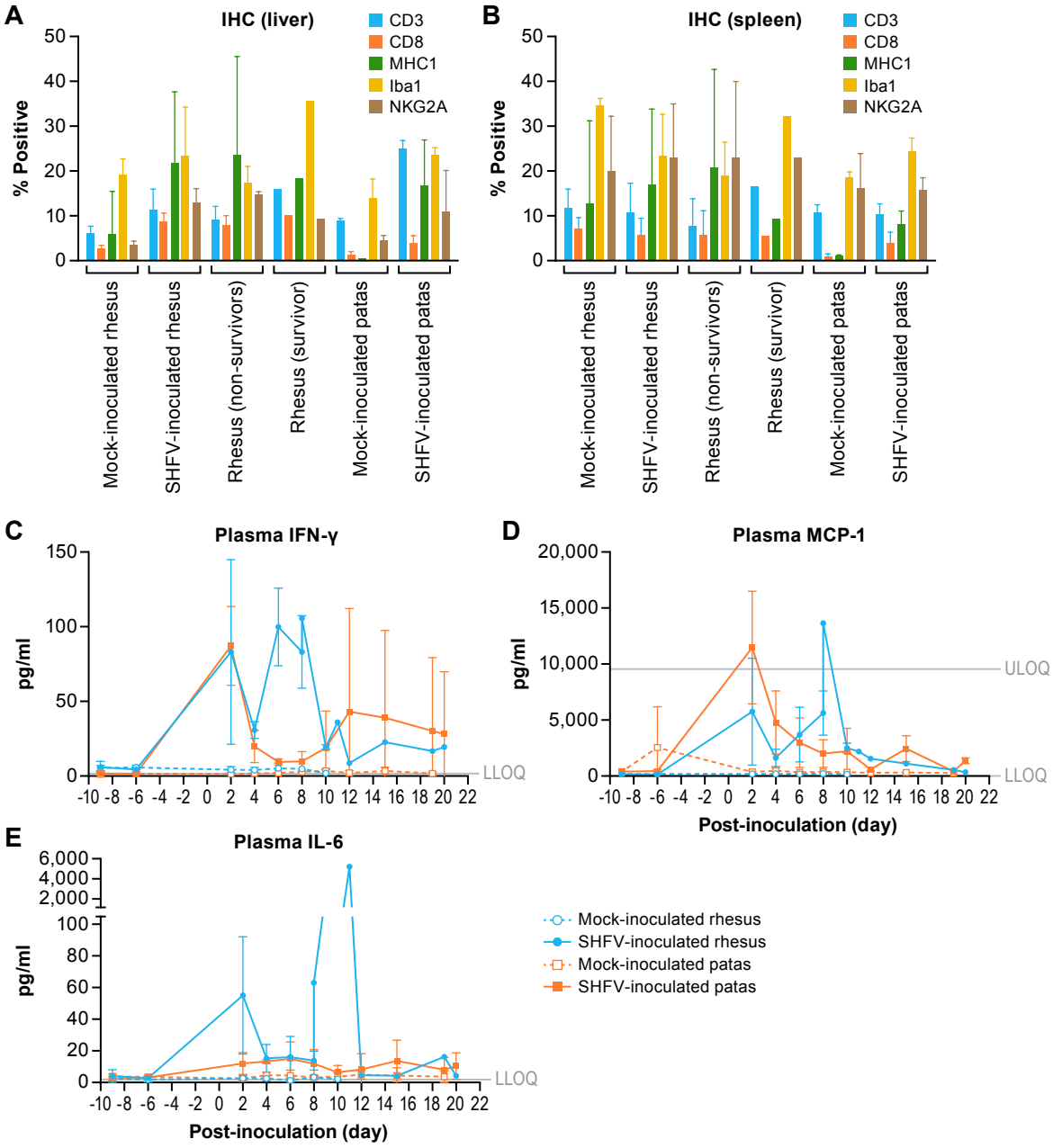


**Figure 4.** Mean quantitative immunohistochemistry values of indicated marker in mock- and SHFV-inoculated patas and rhesus monkey livers and spleens (A, B). Mean plasma concentrations in pg per ml of indicated analyte for mock (open symbols) and SHFV-inoculated (solid symbols) patas (orange) and rhesus (blue) monkeys (C–E). Gray lines represent the lower and upper limits of quantitation (LLOQ and ULOQ, respectively).

Figure 5

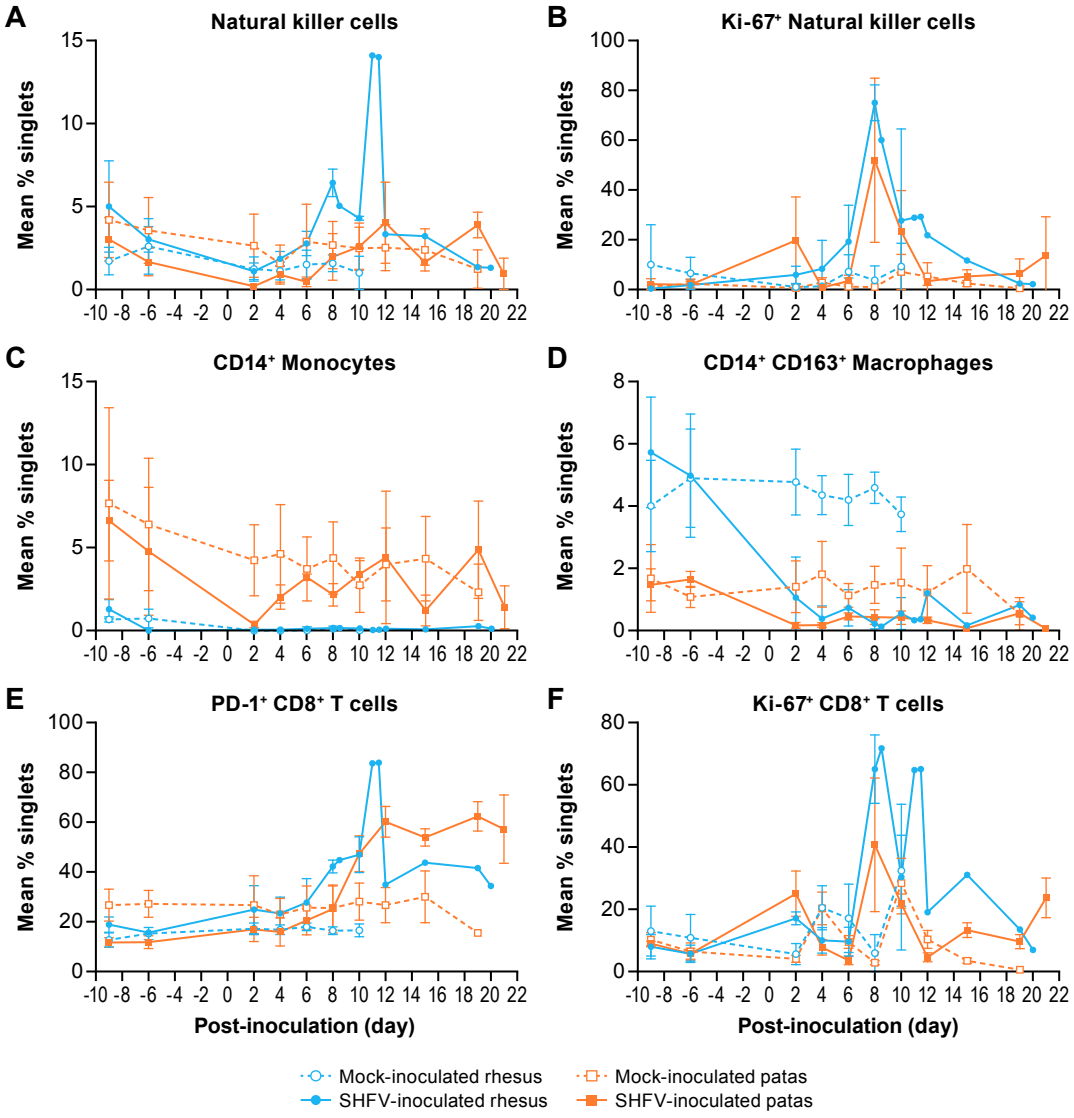


**Figure 5.** Mean percentage of indicated cell populations from whole blood of mock (open symbols) and SHFV-inoculated (solid symbols) patas (orange) and rhesus (blue) monkeys (A-F).

# Figure 6

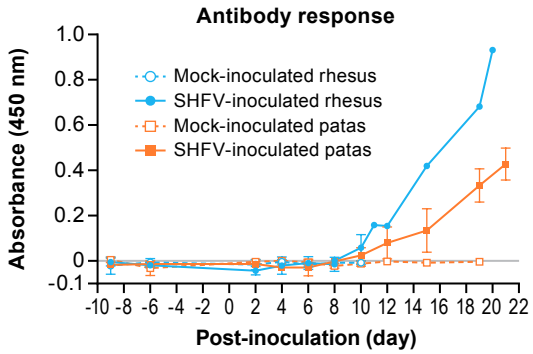


**Figure 6.** Mean ELISA absorbance values for patas (orange lines) and rhesus monkeys (blue lines) either exposed to 5,000 PFU of SHFV (solid symbols) or with PBS (open symbols).